Published in final edited form as:
J Appl Physiol. 2005 November ; 99(5): 1992–1997.

Long-range diffusion of hyperpolarized ^{3}He in explanted normal and emphysematous human lungs via magnetization tagging

Jason C. Woods[1,2], **Dmitriy A. Yablonskiy**[1,2], **Cliff K. Choong**[3], **Kimiaki Chino**[3], **John A. Pierce**[4], **James C. Hogg**[5], **John Bentley**[5], **Joel D. Cooper**[3], **Mark S. Conradi**[1,2], and **Peter T. Macklem**[6]

1 *Department of Physics, Washington University, St. Louis, Missouri*

2 *Department of Radiology, Washington University, St. Louis, Missouri*

4 *Department of Internal Medicine, Washington University, St. Louis, Missouri*

3 *Jacqueline Maritz Lung Center, Washington University, St. Louis, Missouri*

5 *iCAPTURE Center, St Paul's Hospital, Vancouver, British Columbia*

6 *Meakins-Christie Laboratories, McGill University, Montreal, Quebec, Canada*

Abstract

Long-range diffusivity of hyperpolarized ^{3}He gas was measured from the decay rate of sinusoidally modulated longitudinal nuclear magnetization in three normal donor and nine severely emphysematous explanted human lungs. This (long-range) diffusivity, which we call D_{sec}, is measured over seconds and centimeters and is ~10 times smaller in healthy lungs (0.022 cm^2/s) than the more traditionally measured D_{msec}, which is measured over milliseconds and submillimeters. The increased restriction of D_{sec} reflects the complex, tortuous paths required to navigate long distances through the maze of branching peripheral airways. In emphysematous lungs, D_{sec} is substantially increased, with some regions showing nearly the unrestricted value of the self-diffusion coefficient (0.88 cm^2/s for dilute ^{3}He in air, a 40-fold increase). This suggests the presence of large collateral pathways opened by alveolar destruction that bypass the airways proper. This destruction was confirmed by comparison with histology in seven lungs and by removal of trapped gas via holes in the pleural surface in five lungs.

Keywords

emphysema; diffusivity; airways; transplant surgery; alveolar destruction

In recent years, ^{3}He magnetic resonance imaging has been shown to be an effective tool for characterizing lung ventilation and microstructure. Maps of ^{3}He spin density have been used to identify ventilation defects in a variety of lung diseases (11,15), and measurements of restricted diffusion over millisecond time scales have been a powerful probe of emphysema (3,4,20,21,29). Air space expansion and tissue destruction due to emphysema result in fewer and larger air spaces; alveolar walls, which normally restrict gas diffusion, are absent, giving rise to an increase in gas diffusivity (19,25). During a typical experimental diffusion time of 2 ms, most ^{3}He atoms cannot diffuse from one acinar airway (e.g., an alveolar duct) to its neighbor; thus the results are sensitive only to the size and geometry of alveoli and individual alveolar-lined airways within the acinus (8,29).

Address for reprint requests and other correspondence: J. C. Woods, Dept. of Physics, Box 1105, Washington Univ., One Brookings Dr., St. Louis, MO 63130-4899 (e-mail: woods@wuphys.wustl.edu).

Measurements of ^{3}He diffusion over longer times and distances are possible with spatially modulated longitudinal magnetization, because the time constant for relaxation of longitudinal magnetization (T_1) is much longer than the time constant for transverse magnetization (T_2^*): in humans at 1.5 T, T_1 of ^{3}He in lung is ≥20 s and T_2^* is 20 ms (11). Spatial modulation of longitudinal magnetization has been used to monitor cardiac or thoracic motion (1,7,17); in the air spaces of lungs as used here, the motion of ^{3}He is stochastic (diffusive) and results in attenuation of the spatial modulation (16). Diffusion averages across the spatially modulated magnetization, so the diffusivity may be determined from the decay rate of the amplitude of the modulation. Recently, experiments of ^{3}He diffusion over seconds and centimeters via magnetization tagging have shown that the long-range diffusivity (D_{sec}) is very restricted in healthy human and canine lungs: 0.015–0.02 cm^2/s (16,28). These values of D_{sec} are ~10 times smaller than diffusivity measured over 2–5 ms and over submillimeter length scales (D_{msec}) via a variation of the Stejskal-Tanner experiment (20,22). In addition, the average two- to threefold increase of D_{sec} that has been shown in elastase-induced emphysema in dogs is somewhat larger than the increase than D_{msec} in the same animals (28).

Human lungs have, on average, ~24–25 levels of bifurcating airways (8,26). At the tracheal end and extending ~16 branching points into the lung, gas transport is primarily by convection. At the acinar end, from respiratory bronchioles to alveolar ducts and sacs, transport is primarily by diffusive mixing (modified by cardiogenic mixing). At the “diffusion front,” diffusion, convection, and cardiogenic mixing play a role, with the importance of convection progressively diminishing and diffusion increasing with increasing branching number (18). We are concerned only with diffusion in the gas spaces, not diffusion across alveolar-capillary membranes, as is most often discussed. All gases within this diffusive (respiratory) zone are transported to and from alveolar boundaries according to their respective free diffusion coefficients (D_o) (18).

All these bifurcating pathways are singly connected; i.e., there is only one route between any two points in a healthy lung. Collateral ventilatory pathways, consisting of canals of Lambert and collateral alveolar ducts (12,13), provide an alternate route for some gas atoms to travel from alveoli in one acinus to another, but in a healthy lung they are relatively unimportant physiologically (23). Because the alveoli and acinar airways, which occupy most of the lung volume and, therefore, are responsible for nearly all the ^{3}He magnetic resonance signal, are no more than only a few millimeters long, diffusion over ≥1 cm (from one acinus to its neighbor) requires that the gas negotiate the mazelike airway network, likely going up and down several levels of branching. Because of the tortuous nature of the airway paths over these distances, D_{sec} is substantially smaller than diffusion measured while atoms are confined to single small airways, i.e., D_{msec} (16,28). (Because ^{3}He is virtually insoluble in tissue, diffusion across barriers is not considered.)

Collateral ventilation paths, which are relatively unimportant in health but are very significant in emphysema (9,12,23), are defined as all pathways other than the airways proper. The tissue destruction that characterizes emphysema creates new collateral channels that become important, low-resistance ventilatory pathways (13,23). Emphysematous destruction of acinar parenchyma opens direct pathways between points in the parenchyma that were previously connected only by long tortuous channels, which should result in marked increases in D_{sec}. Moreover, the ratio of D_o (0.88 cm^2/s for dilute ^{3}He in air or N_2) to restricted diffusivity in healthy lungs is ~10 times larger for D_{sec} than for D_{msec}: 0.88:0.02 vs. 0.88:0.20. Thus the possible fractional increase is 10 times larger in D_{sec} than in D_{msec}, which could make D_{sec} a more sensitive probe of emphysema than D_{msec}.

In this study, we test the hypothesis that the alveolar destruction that characterizes emphysema allows more rapid long-range diffusion between acini and lobules than in normal lungs. Although parenchymal destruction presumably also creates the low-resistance collateral pathways that were described over a quarter of a century ago in emphysema (9), we made no attempt to prove that the pathways for long-range diffusion were identical to collateral ventilation conduits. To test our hypothesis, we measured spatially resolved long-range ^{3}He diffusion via the decay of spatially modulated longitudinal ^{3}He magnetization in normal lungs rejected for transplantation because of recipient mismatch and explanted emphysematous human lungs removed at transplant surgery. We also correlated the restricted D_{sec} with quantitative histological measurements of surface area-to-volume ratios (SA/V) in individual samples of lung tissue.

Previous studies of the mechanical and diffusive properties of excised and intact, living animal lungs (5,27) suggest that they should be similar to lungs in living humans in our experiments, except for the absence of cardiogenic mixing, which tends to accelerate diffusive mixing. Because we report abnormally rapid long-range diffusive mixing in the absence of convection in emphysematous lungs, the effect of the heart and convection through collateral channels with breathing would be to magnify this abnormality even further.

All the present experiments are possible in vivo and have been successfully conducted in dogs (28). We used explanted lungs, which enabled us to determine whether alveolar destruction correlated with the rapid long-range diffusion we found in emphysematous lungs. The normal lungs served as controls. Furthermore, by studying lungs with the real anatomic pathology of emphysema, rather than an animal or structural model, we approached conditions similar to those in living patients with chronic obstructive pulmonary disease. Explanted lungs also have advantages for the study of disease: regions that would not be well ventilated within a single breath can be fully ventilated by repeated breaths, and the depolarizing effects of O_2 can be avoided (19). We show here that D_{sec} in three normal human donor lungs is very restricted, in agreement with previous measurements, and that D_{sec} is very significantly increased in severely emphysematous lungs removed at transplant surgery.

MATERIALS AND METHODS

Nine severely emphysematous lungs were removed at transplant surgery and stored loosely wrapped in a towel moistened with saline at 40°F for 2–5 days before imaging. Three normal donor lungs that were rejected for transplantation because of recipient mismatch were stored similarly and used as controls; one donor (40-yr-old *Control 2R* in Table 1) had a smoking history of 20 pack · yr. Storage of the lungs for this period of time did not affect their quality for quantitative histology. These studies were performed with the approval of the Institutional Review Board.

In one control and five emphysematous lungs, tubes glued to the visceral pleura communicated directly with the lung parenchyma via an incision in the pleural surface; this subset of lungs was part of a much larger study of transpleural ventilation, a therapeutic approach originally suggested by Macklem (13). The tubes did not affect the diffusion measurements, because these measurements were not made in close proximity to the tubes (which were closed during imaging experiments) and because most of the parenchyma was unaffected. We did, however, assess passive gas expiration and trapped gas removal through the transpleural conduits via a pneumotachometer and by water displacement, respectively, in this subset of lungs. After the lungs passively deflated through the bronchus from 10 cmH_2O transpleural pressure, we measured the volume of total gas expiration through the pleural tube when it was open via a pneumotachometer. We also measured the volume of water displaced by the lungs after passive deflation before and after the pleural tube was open for 15 s.

Before imaging, leaks in the lungs were sealed and the lungs were purged with 100% N_2 via an open-circuit technique. The lungs were placed in the magnetic resonance scanner, inflated to approximately functional residual capacity with N_2, and then ventilated using a syringe containing ~300 ml of ^{3}He. After at least three 300-ml rebreathing strokes with the syringe to mix ^{3}He with N_2 in the lung, imaging with magnetization tagging was performed at end inspiration. By using very small flip angles, substantial ^{3}He magnetization remained for the magnetization-tagged, D_{sec} measurements reported here.

Hyperpolarized ^{3}He of 40% absolute polarization was prepared with one commercial (General Electric) and two home-built polarizers to allow as many as six separate 300-ml boli of gas for an imaging session. A home-built, solenoid-like radio frequency (rf) coil took advantage of the lack of tissue around the lungs, resulting in low rf loss (Q = 80) and correspondingly high signal-to-noise ratio (SNR). A Siemens Magnetom Vision whole body imager was used at 48.47 MHz. The high-Q coil required retuning before each experiment but provided high SNR and a homogeneous rf field.

Sinusoidal modulation of ^{3}He magnetization with wavelength λ was achieved after the final ventilation cycle by two 45° rf pulses separated by a gradient pulse of amplitude G and effective duration t, such that $\gamma G\lambda t = 2\pi$, where γ is the gyromagnetic ratio of the ^{3}He nucleus. The resulting longitudinal magnetization is modulated as follows: $M(x) = [1 - \cos(\gamma Gtx)]/2$ (28). The use of 45° pulses yields 100% modulation while avoiding negative magnetization, which would be misreported in the magnitude value, gradient-echo images used here. The magnetization tagging had wavelengths of 2.0 and 3.0 cm, which were chosen to yield a significant, but not complete, decay of the modulation after several seconds. In normal donor lungs, where much less diffusion and modulation decay were expected, the smaller wavelength was used. After tagging, 4–15 subsequent FLASH image sets (3° flip angle) in approximately axial or sagittal planes (defined by the lung's normal orientation in the body) inspected the decaying modulation. Fewer FLASH images were used per slice if more slices were acquired. The 20-mm-thick slices were 320-mm field of view, with 5 × 2.5 mm pixels; better resolution was in the read-out direction, normal to the tagging planes, and in the direction along which diffusion is probed. In three cases, measurements were made in multiple diffusion directions: anterior↔posterior and medial↔lateral. As many as nine total slices were imaged, although higher time resolution with fewer slices was needed when the decay was particularly fast; six of the emphysematous lungs necessitated imaging of only one slice at a time. For comparison, maps of the short-range ^{3}He diffusivity (D_{msec}) were generated by the ratio of two interleaved, gradient-echo FLASH images, with $b = 0$ and 1.375 s/cm^2 (b is a measure of gradient strength and duration; diffusion time = 1.8 ms) (20), using the same field of view as for D_{sec}, but with 5 × 5-mm resolution.

D_{sec} was measured for each pixel from the decay rate constant (R) of the fractional sinusoidal modulation FM(x), which is defined below as a discrete Fourier sum involving only neighboring pixels over one tagging wavelength in the read-out direction. Cosine and sine components [C(x) and S(x), respectively] of the image intensity data [I(x)], in addition to the average [a(x)], were calculated for each image as follows (28)

$$a(x) = \sum_{\Delta x} I(x + \Delta x) \tag{1}$$

$$C(x) = \sum_{\Delta x} I(x + \Delta x) \cos\left[\frac{2\pi(x + \Delta x)}{\lambda}\right] \tag{2}$$

$$S(x) = \sum_{\Delta x} I(x + \Delta x) \sin\left[\frac{2\pi(x + \Delta x)}{\lambda}\right] \tag{3}$$

$$FM(x) = \frac{\sqrt{C(x)^2 + S(x)^2}}{a(x)} \quad (4)$$

All sums are over Δx, from $-\lambda/2$ to $\lambda/2$, with no end-point redundancy. Because FM is defined as the ratio in Eq. 4, it is unaffected by uniform T_1 decay and consumption of the magnetization by rf pulses (see Fig. 1 in Ref. 28) but is sensitive to the apparent diffusivity of the gas. If we consider a simplified situation where the longitudinal magnetization [$M(x)$] at $t \geq 0$ is characterized purely by the cosine function, then at $t = 0$, $M(x,0) = \frac{1}{2}[1 - \cos(kx)]$, where $k = 2\pi/\lambda$. The pertinent solution to the diffusion equation, with T_1 relaxation included, is $M(x,t) = e^{-t/T_1}[1 + e^{-Rt}\cos(kx)]$, where R is given by $4\pi^2 D_{sec}/\lambda^2$ (14). The fractional modulation then decays with time according to Eq. 4: $FM(x,t) = \frac{1}{2}e^{-Rt}$. Maps of D_{sec} are generated from the exponential decay rate constant R of the fractional modulation $FM(x,t)$ at each pixel as follows: $R = 4\pi^2 D_{sec}/\lambda^2$ (14); in practice, this is achieved by fitting FM at each pixel to an exponential decay with time. Even though Eqs. 1–4 provide data for each Δx and give a smooth presentation of the maps of D_{sec}, the true resolution of the maps is closer to $\lambda/2$.

We froze, sampled, and preserved tissue from one normal and six diseased lungs for quantitative histological studies. After imaging, these lungs were inflated to 10 cmH_2O pressure and frozen in cold (77–100 K) N_2 vapor. The entire frozen specimen was then cut into 2-cm-thick transverse slices, placed on dry ice, and randomly sampled using a cork borer, with 15–20 samples per lung, at recorded locations. These samples were fixed in 70% alcohol at −40°C and then shipped to the iCAPTURE Center, where they were processed into paraffin blocks. Sections (4 – 6 μm thick) were cut from these paraffin blocks and stained with hematoxylin and eosin. Each section was randomly sampled with at least five microscope fields using a ~10 objective lens. Point and intercept counts were collected using the “multipurpose test system” proposed by Weibel (24). The surface density and SA/V were calculated first manually and later using Image Pro Plus (Media Cybernetics) image analysis software, which was validated against the manual method. We were able to approximately match 59 individual histological samples to image regions in maps of D_{sec} for comparison and validation. Image slices of D_{sec} and physical cutting of the frozen lungs were in different orientations, so the matching of image positions to the sampled tissue has an approximate uncertainty of ±1 cm.

RESULTS

N_2 purge removed almost all the O_2, so the T_1 of ^3He was much longer than the total experiment time, which is on the order of 100 s. If the lung contained 1% air (0.2% O_2), T_1 of ^3He due to O_2 alone would be ~17 min (19). In two cases, T_1 was measured directly to be 7–9 min, suggesting that a small amount of air had entered through leaks or that there was significant wall relaxation. Virtually all areas in each lung received enough gas for the diffusion measurements after repeated breaths. SNR in the images was as high as 150 and never <10. Ex vivo improvements in SNR are ~12 dB over those in vivo because of the increased Q and superior filling factor (28). Near-complete tagging modulation (with minima <10% of maxima) was realized in all cases.

In the three normal lungs, D_{sec} was very restricted ($D_{sec} = 0.022$ cm^2/s) in nearly all parts of the multiple slices imaged, which together cover most of each lung (Fig. 1). After ~3 s of decay, only small changes in the sinusoidal modulation are evident; the resultant map of long-range diffusivity reports low and generally uniform values. In all three control lungs, there were regions of slightly enhanced D_{sec} without accompanying enhancement of D_{msec} in the same regions.

A wide distribution of D_{sec} was measured in the severely emphysematous lungs. The average D_{sec} across these lungs was 0.24 cm^2/s, an 10-fold increase compared with the control lungs.

In every case, there was marked heterogeneity of D_{sec} compared with the control lungs (Fig. 2), with many regions of greatly enhanced diffusion (e.g., D_{sec} >0.4 cm^2/s), particularly in the upper lobes. Data from all lungs are summarized in Table 1.

Diffusion was often so rapid that decay of spatially modulated magnetization was obvious in the raw images (Figs. 2 and 3). Some regions with D_{sec} near the unrestricted value were detected, representing an ~40-fold increase in diffusivity compared with normal lung (Fig. 3). Comparison of the maps of D_{sec} with the maps of D_{msec} shows distinct qualitative differences. Examples include the regions of enhanced D_{sec}, whereas D_{msec} is comparatively uniform, in the normal lungs in Fig. 1. In Fig. 3, the map of D_{sec} shows substantial variation across the lung, with some restriction to diffusion in the upper lobe, in contrast to the uniform and nearly unrestricted values of D_{msec} (D_{msec} has saturated near the value of D_o = 0.88 cm^2/s).

Even though image sets of D_{sec} did not cover the entire lung, we matched regions in these images to samples for which quantitative histology had been performed (Fig. 4, with averages in Table 1). Despite the imprecision (±1 cm) in matching regions of D_{sec} maps with those where SA/V was measured, the correlation (Fig. 4) between SA/V and D_{sec} in the samples for which we were able to match the two measures shows a significant, nonlinear, inverse relation. An equation of reasonable fit is presented in Fig. 4.

Trapped gas volume was four times greater in explanted emphysematous lungs than in control lungs: 2.0 ± 1.1 vs. 0.5 ± 0.2 liter. We recovered 60 ± 42% of the trapped gas volume via the transpleural conduits. There was a rough, linear correlation between the percentage of trapped gas removed and the average D_{sec} (r^2 = 0.77) for the five emphysematous lungs.

DISCUSSION

The ^{3}He closed-circuit rebreathing procedure (after open-circuit purging of O_2 by 100% N_2) described here results in reasonably uniform gas distribution, even in portions of emphysematous lungs that do not receive much gas during single inspirations. This technique distributes ^{3}He throughout the lung with little or no depolarization by O_2. This ensures that images of the decay of modulated magnetization completely cover the lung, allowing diffusivity to be measured under static conditions even in the most diseased regions. Previous ^{3}He magnetic resonance images in vivo typically show one or more regions of inadequate ventilation where the diffusivity cannot be determined (20). Although repetitive rebreathing of an anoxic gas mixture (as used here) cannot be repeated in vivo, a more modest rebreathing procedure (i.e., the rebreathing method used to measure functional residual capacity by He dilution) could be effective at obtaining better results in humans with abnormal ventilation distributions.

The result of D_{sec} = 0.022 cm^2/s in the control lungs is consistent with results from a previous study of in vivo human lungs (15,16) and a study of healthy dog lungs (28) in which similar values of D_{sec}, i.e., ~1/40th of D_o, were found. By contrast, in several of the explanted emphysematous lungs examined here, regions of very large D_{sec} were present, with 25- to 40-fold increases relative to the 0.022 cm^2/s average of the normal donor lungs. This is consistent with our calculation (see above) that the possible fractional increase in D_{sec} is an order of magnitude greater than that for D_{msec}.

The correlation of D_{sec} with SA/V (Fig. 4) strongly suggests that the areas of unrestricted D_{sec} are indeed regions of extreme tissue destruction. In all likelihood, these are the trapped gas regions that communicated with the transpleural conduits but not with the tracheobronchial tree. In smoking-induced emphysema, the worst disease is commonly found in the upper lobes (25), in agreement with the location of the areas of largest D_{sec} in Figs. 2 and 3, and in five of the other seven emphysematous lungs. However, SA/V and D_{sec} measure very distinct aspects

of the lung: SA/V is determined from a 10-μm histological section of a 2-cm-long core of tissue, and D_{sec} is determined from a volume-averaged image of regional acinar connectivity. Long-range diffusion seems particularly sensitive for lungs with SA/V ≤120 cm^{-1}, where tissue sampling and morphometry become difficult for practical reasons. Therefore, for us, the immediate utility of D_{sec} appears to be in quantifying advanced emphysema.

To execute a net displacement of approximately $\lambda/2$ (here 1.0–1.5 cm) and with the assumption that ^{3}He cannot penetrate the airway and alveolar walls (He is only very slightly soluble), the tortuous nature of the branching airways requires a ^{3}He atom to diffuse a much longer path than $\lambda/2$ (2). Thus one expects D_{sec} to be much smaller than D_o or even D_{msec}, in agreement with the present results in normal lungs. In healthy lungs, as discussed above, diffusion of gas from one acinus to another involves the gas moving up and then down several airway generations, including branches within the acinus (8,23,26). In emphysema, collateral pathways resulting from alveolar destruction allow gas to flow more easily through the parenchyma than through the tracheobronchial tree (9,13). Thus the presence of collateral pathways offers a larger number of more direct diffusion paths, so D_{sec} is increased (23). We note that different tagging wavelengths may lead to different apparent diffusivities in the same lung, because the length scale and tortuosity of lung architecture will be different. Thus, for increasing wavelengths in healthy lungs, we expect D_{sec} to decrease, because atoms must negotiate a more tortuous path, but this decrease has not been observed in the length-scale studies by us and others (16). In emphysematous lungs, the relation between D_{sec} and λ will depend on the extent of the collateral pathways.

The increased collateral communication is directly evidenced in this study by the increased expiratory flow and trapped gas removal via transpleural conduits compared with the airways in the subset of lungs with external tubes through the pleural surface. The trapped gas that could be removed via these conduits showed that collateral channels communicated with a larger volume of the lung parenchyma than did the tracheobronchial tree. For relief of lung mechanical abnormalities and gas trapping in emphysematous lungs, surgical construction of artificial airways directly through the rib cage and visceral pleura into the lung parenchyma, bypassing obstructed airways, has been proposed (13). A better approach might be construction of fenestrations through the bronchial wall into the lung parenchyma (10). All such new therapeutic approaches will depend on good collateral ventilation, so that large volumes of lung benefit from a small number of these fenestrations. That is, these methods rely on collateral ventilation to remove trapped gas from a substantial volume of hyperinflated lung tissue. Measurement of D_{sec} may be important in determining the extent of tissue destruction, resulting in new collateral pathways and the likelihood of success of the newly proposed remedies in individual patients.

In conclusion, we have taken advantage of the high spin sensitivity in excised lungs and the reasonably uniform gas distribution that can be produced by rebreathing, even in the most diseased regions of lung, in our report of hyperpolarized ^{3}He magnetic resonance imaging in three control and nine severely emphysematous explanted human lungs. D_{sec} was measured by monitoring the decay of sinusoidally modulated longitudinal magnetization. Normal human donor lungs show very restricted D_{sec}, ~1/40th of the free gas diffusivity, reflecting the long and indirect paths along the tortuous airway network between distant points. There was a significant correlation between histological quantification of parenchymal tissue destruction as assessed by SA/V and D_{sec}. Thus we provide strong evidence in favor of our hypothesis that emphysematous alveolar destruction allows more rapid long-range diffusion between acini and lobules than in normal lungs. The measurements of D_{sec} provide very large contrast between normal and severely emphysematous lungs, with increases that are as large as a factor of 40. In addition, D_{sec} reveals significant regional differences in some lungs with nearly uniform,

unrestricted D_{msec}. Measurements of D_{sec} may be particularly useful for characterizing the collateral ventilation pathways that become important in severe emphysema.

Acknowledgements

We are very grateful to the transplant recipients and lung donors' families who allowed this research to take place. We thank the personnel of the transplant program at Washington University.

GRANTS

Research funding was provided by Washington University and National Heart, Lung, and Blood Institute Grants R01 HL-070037 and R01 HL-62194.

References

1. Alex L, Dougherty L. MR imaging of motion with spatial modulation of magnetization. Radiology 1989;171:841–845. [PubMed: 2717762]
2. Bear, J. Dynamics of Fluids in Porous Media. New York: American Elsevier; 1972. p. 109-113.
3. Chen XJ, Hedlund LW, Möller HE, Chawla MS, Maronpot RR, Johnson GA. Detection of emphysema in rat lungs by using magnetic resonance measurements of ^{3}He diffusion. Proc Natl Acad Sci USA 2000;97:11478–11481. [PubMed: 11027348]
4. Chen XJ, Möller HE, Chawla MS, Cofer GP, Driehuys B, Hedlund LW, Johnson GA. Spatially resolved measurements of hyperpolarized gas properties in the lung in vivo. I. Diffusion coefficient. Magn Reson Med 1999;42:721–728. [PubMed: 10502761]
5. Engel LA, Macklem PT. Gas mixing and distribution in the lung. Int Rev Physiol 1977;14:37–82. [PubMed: 321391]
6. Fukushima, E.; Roeder, SBW. Experimental Pulse NMR, a Nuts and Bolts Approach. Reading, MA: Addison-Wesley; 1981. p. 386-387.
7. Groot Koerkamp MAM, Snoep G, Muijtjens AMM, Kemerink GJ. Improving contrast and tracking of tags in cardiac magnetic resonance images. Magn Reson Med 1999;41:973–982. [PubMed: 10332881]
8. Haefeli-Bleuer B, Weibel ER. Morphometry of the human pulmonary acinus. Anat Rec 1988;220:401–414. [PubMed: 3382030]
9. Hogg JC, Macklem PT, Thurlbeck WM. The resistance of collateral channels in excised human lungs. J Clin Invest 1969;48:421–431. [PubMed: 5773080]
10. Lausberg HF, Chino K, Patterson A, Meyers BF, Toeniskoetter PD, Cooper JD. Bronchial fenestration improves expiratory flow in emphysematous lungs. Ann Thorac Surg 2003;75:393–398. [PubMed: 12607646]
11. LeaWoods JC, Yablonskiy DA, Saam B, Gierada DS, Conradi MS. Hyperpolarized ^{3}He gas production and MR imaging of the lung. Concepts Magn Reson 2001;13:277–293.
12. Macklem PT. Airway obstruction and collateral ventilation. Physiol Rev 1971;51:368–436. [PubMed: 4928122]
13. Macklem PT. Collateral ventilation. N Engl J Med 1978;298:49–50. [PubMed: 618452]
14. Mathews, J.; Walker, RL. Mathematical Methods of Physics. Menlo Park, CA: Benjamin; 1970. p. 217-252.
15. Möller HE, Chen XJ, Saam B, Hagspiel KD, Johnson GA, Altes TA, de Lange EE, Kauczor HU. MRI of the lungs using hyperpolarized noble gases. Magn Reson Med 2002;47:1029–1051. [PubMed: 12111949]
16. Owers-Bradley, JR.; Bennattayalah, A.; Fichele, S.; McGloin, JC.; Bowtell, R.; Morgan, PS.; Moody, AR. Diffusion and tagging of hyperpolarized ^{3}He in the lungs. Proc 10th Annual Meeting International Society for Magnetic Resonance in Medicine; Honolulu, Hawaii. 2002. p. 2016
17. Owers-Bradley JR, Fichele S, Bennattayalah A, McGloin CJS, Bowtell RW, Morgan PS, Moody AR. MR tagging of human lungs using hyperpolarized ^{3}He gas. J Magn Reson Imaging 2003;17:142–146. [PubMed: 12500284]

18. Paiva M, Engel LA. Pulmonary interdependence of gas transport. J Appl Physiol 1979;47:296–305. [PubMed: 224024]
19. Saam BT, Happer W, Middleton H. Nuclear relaxation of ^{3}He in the presence of O_2. Phys Rev A 1995;52:862–865. [PubMed: 9912313]
20. Saam B, Yablonskiy DA, Kodibagkar VD, Leawoods JC, Gierada DS, Cooper JD, Lefrak SS, Conradi MS. MR imaging of diffusion of ^{3}He gas in healthy and diseased lungs. Magn Reson Med 2000;44:174–179. [PubMed: 10918314]
21. Salerno M, de Lange EE, Altes TA, Truwit JD, Brookeman JR, Mugler JP. Emphysema: hyperpolarized helium 3 diffusion MR imaging of the lungs compared with spirometric indexes—initial experience. Radiology 2002;222:252–260. [PubMed: 11756734]
22. Stejskal EO. Use of spin echoes in a pulsed magnetic-field gradient to study anisotropic restricted diffusion and flow. J Chem Phys 1965;43:3597–3603.
23. Terry PB, Traystman RJ, Newball HH, Batra G, Menkes HA. Collateral ventilation in man. N Engl J Med 1978;298:10–15. [PubMed: 618444]
24. Weibel, ER. Stereologic Methods. London: Academic; 1979. p. 9-196.
25. West, JB. Pulmonary Pathophysiology. 4. Baltimore, MD: Williams & Wilkins; 1992. p. 58-62.
26. West, JB. Respiratory Physiology. 5. Baltimore, MD: Williams & Wilkins; 1995. p. 21-30.
27. Wohl ME, Turner J, Mead J. Static pressure-volume curves of dog lungs in vivo and in vitro. J Appl Physiol 1968;24:348–354. [PubMed: 5640721]
28. Woods JC, Yablonskiy DA, Chino K, Tanoli TSK, Cooper JD, Conradi MS. Magnetization tagging decay to measure long-range ^{3}He diffusion in healthy and emphysematous canine lungs. Magn Reson Med 2004;51:1002–1008. [PubMed: 15122683]
29. Yablonskiy DA, Sukstanskii AL, LeaWoods JC, Gierada DS, Bretthorst GL, Lefrak SS, Cooper JD, Conradi MS. Quantitative in vivo assessment of lung microstructure at the alveolar level with hyperpolarized ^{3}He diffusion MRI. Proc Natl Acad Sci USA 2002;99:3111–3116. [PubMed: 11867733]

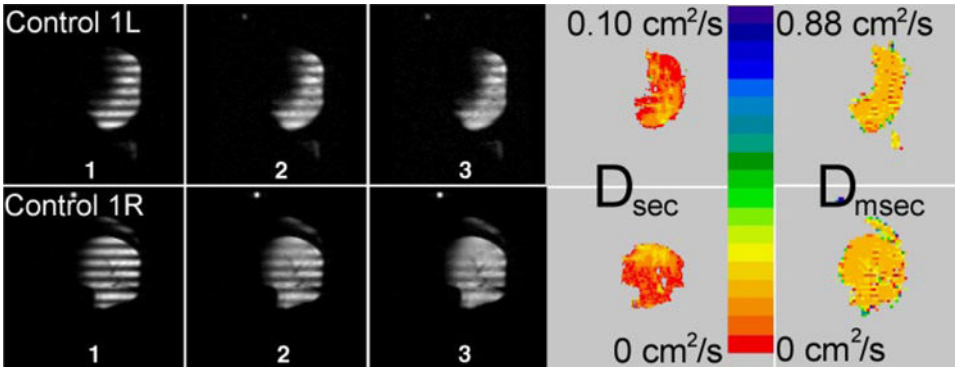

Fig. 1.

Sequence of time-evolving, modulated ^{3}He magnetization in approximately transverse slices (lateral is at *right* of both images) from 2 normal human donor lungs. Gray-scale *images 1–3* advance 2.9 s per frame; tagging wavelength is 2 cm. Images of long-range diffusion (D_{sec}) were calculated from gray-scale images; short-range diffusion (D_{msec}) is shown for comparison. D_{sec} is substantially different from D_{msec}, with D_{sec} lower than D_{msec} by a factor of ~10: D_{sec} = 0.021 cm^2/s and D_{msec} = 0.21 cm^2/s. Scales for D_{sec} and D_{msec} differ by a factor of 8.8.

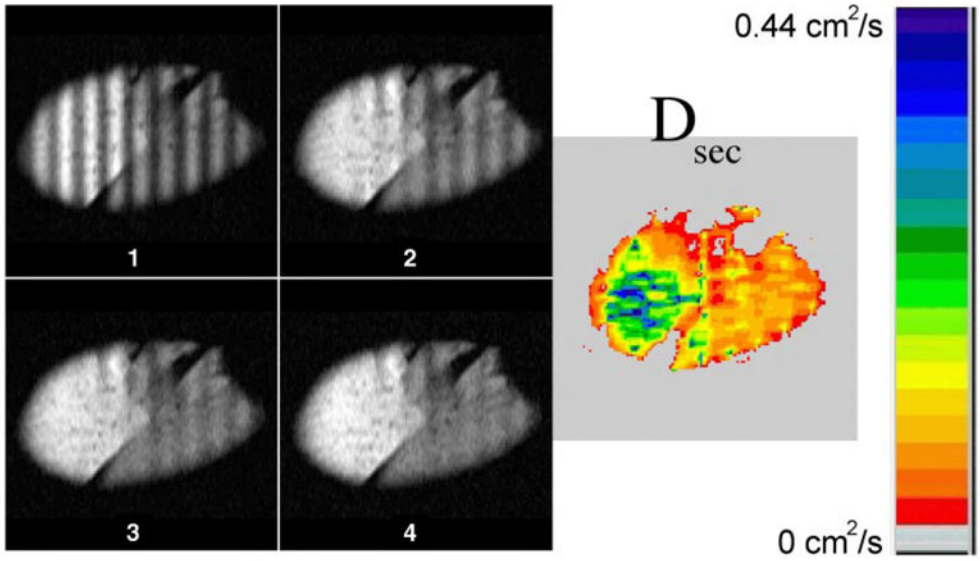

Fig. 2.

Gray-scale *images 1–4* advance in time by 1.96 s per frame for an emphysematous left lung removed at transplant. Images are approximately sagittal, with a 3-cm tagging wavelength. Diffusion map calculated from decay of sinusoidal modulation is displayed in color (*right*); a large region in the upper lobe (*left*) reaches >0.4 cm^2/s. Attenuation of the modulation is obvious in *image 2* and is faster in the upper lobe. Note different scale from Fig. 1.

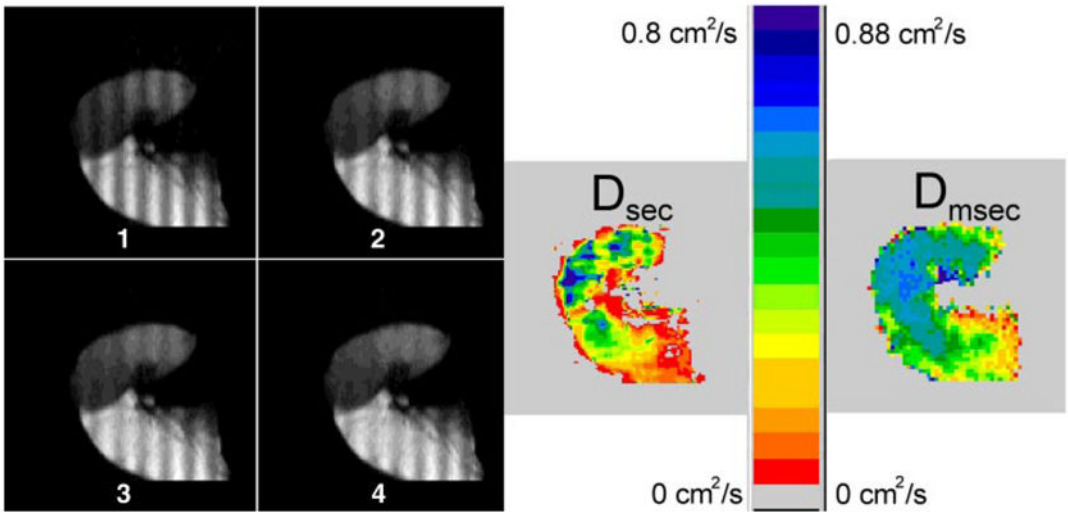

Fig. 3.

Sequence of approximately sagittal *images 1–4* from a severely emphysematous explanted left lung; each frame advances only 0.4 s. Washout of the modulation is particularly rapid and is apparent in the later images. Upper lobe (*left* and *top* of images) has regions of nearly unrestricted diffusion in the map of D_{sec}, yet it still shows some regional variation. D_{msec} map, calculated from a different image set, is nearly saturated at D_o in the upper lobe.

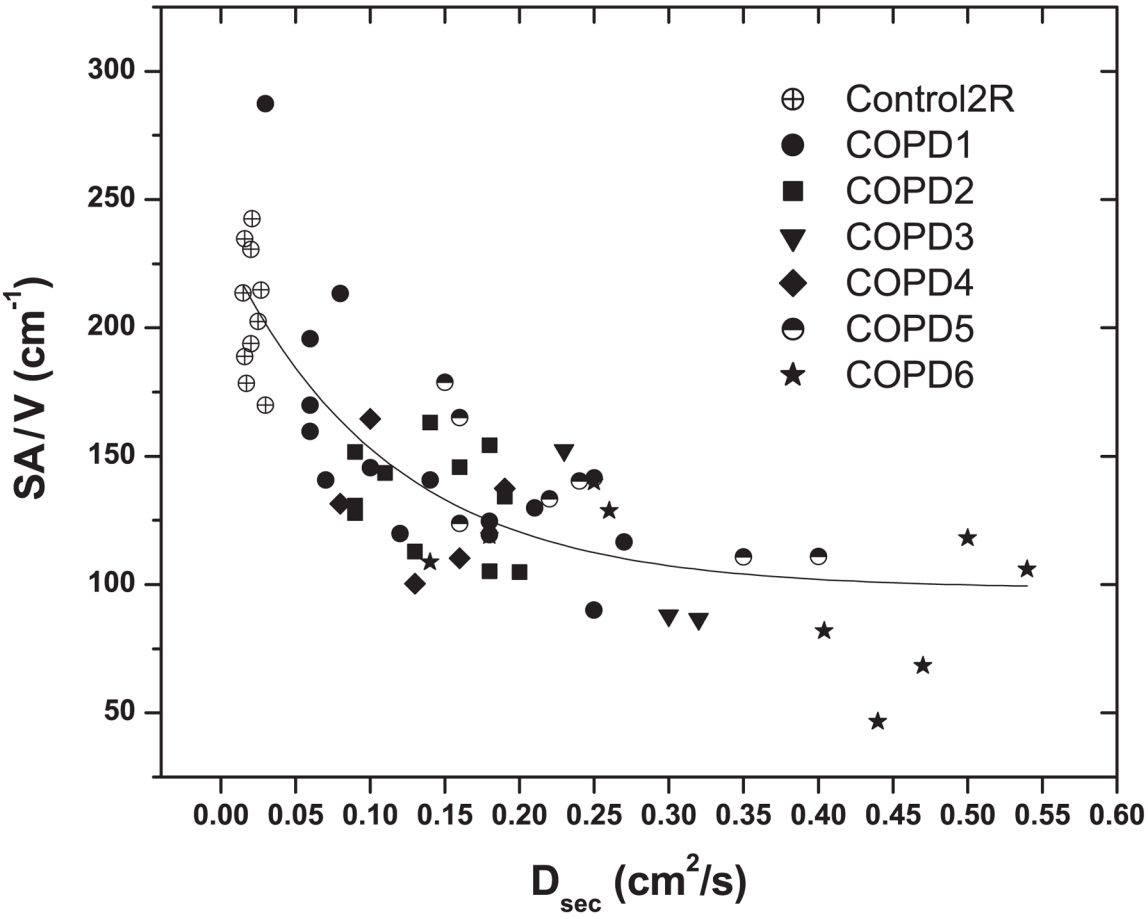

Fig. 4.

Comparison of morphometry [ratio of surface area to volume (SA/V)] and D_{sec} for 59 individually matched samples from 1 control and 6 emphysematous lungs. Relation is inverse and nonlinear. Empirical fitting is as follows: SA/V = 98 + 131 exp(−9 D_{sec}), with r^2 = 0.67 (units in cm · g · s). COPD, chronic obstructive pulmonary disease.

Table 1

^{3}He D_{sec} measurements in normal donor lungs and lungs with end-stage COPD removed at transplant

	SA/V, D_{sec},±σ, cm^2/s cm^{-1}				
	cm^{-1}	**A↔P**	**M↔L**	**λ, cm**	***n***
Control1L		0.024±0.015	0.022±0.015	2	9,9
Control1R		0.024±0.013	0.020±0.014	2	9,9
Control2R	202	0.017±0.015		2	4
COPD1	153	0.16±0.13		3	1
COPD2	138	0.22±0.18		3	3
COPD3	134	0.29±0.2		3	1
COPD4	141	0.11±0.06		3	6
COPD5	141	0.22±0.19		3	2
COPD6	101	0.34±0.15		3	3
COPD7		0.46±0.33	0.41±0.25	3	2,2
COPD8		0.29±0.15		3	2
COPD9		0.091±0.090		3	3
Avg control	202	0.022±0.015	0.021±0.015	2	
Avg COPD	135	0.24±0.16		3	

D_{sec} and σ, average restricted diffusivity measured over seconds with magnetization tagging and its standard deviation across all pixels, respectively; A↔P and M↔L, diffusion measured in anterior↔posterior and medial↔lateral directions, respectively; COPD, chronic obstructive pulmonary disease; λ, wavelength, *n* number of slices. Ratio of surface area to volume (SA/V) was measured morphometrically in 1 normal and 6 emphysematous lungs (*COPD1*-*COPD6*) and is shown for comparison.